International Journal of ENGINE RESEARCH

Standard Article

International J of Engine Research
2017, Vol. 18(10) 1017–1034

DOI: 10.1177/1468087417697759
journals.sagepub.com/home/jer
SAGE

Effects of cavitation in common-rail diesel nozzles on the mixing process

J Javier López[1], Oscar A de la Garza[2], Joaquin De la Morena[1] and S Martínez-Martínez[2]

Abstract

A study to experimentally analyze the effect of cavitation on the mixing process in diesel nozzles was carried out. The mixing process was studied through the spray cone angle. It was characterized in two different scenarios: with the liquid length (nearly realistic conditions, that is, evaporative but non-reactive spray) and the heat release fraction (fully realistic conditions, that is, evaporative and reactive spray). In both studied scenarios, the increase in spray cone angle caused by the cavitation phenomenon, which leads to a better mixing process, has been confirmed. Nevertheless, when the variations of the effective injection velocity and the spray cone angle obtained by comparing a cylindrical nozzle (i.e. a nozzle that promotes the cavitation phenomenon) with a conical nozzle (i.e. a nozzle that inhibits this phenomenon) were analyzed together, it was found that, for the cases studied here, the mixing process worsens with the cylindrical nozzle.

Keywords

Diesel nozzle, cavitation, injection process, spray cone angle, combustion process

Date received: 25 May 2016; accepted: 23 January 2017

Introduction

Among the ways to fulfill the requirements of customers and the legislations regarding pollutant emissions, the design of the nozzle geometry in a diesel engine is an important factor to improve the combustion process. It might lead to a reduction of the pollutant emissions, as demonstrated by Karra and Kong[1] and Som et al.[2] These authors showed that the nozzle geometry has a significant impact on soot emissions. This can be explained by the influence of the nozzle geometry on the internal flow and the characteristics of the spray, especially on the atomization and mixing processes. In fact, this is the main reason why many studies, such as Payri et al.,[3] Wang et al.,[4] Som et al.,[2] Watanabe et al.[5] and Hayashi et al.[6] have analyzed the effect of the nozzle geometry on the internal flow and the characteristics of the spray.

One of the most significant aspects in this sense is the formation of cavitation inside the nozzle. This cavitation can appear in different zones of the nozzle depending on the flow condition. First, cavitation can be induced due to the flow separation at the nozzle orifices inlet, where the pressure drop can decrease significantly when high flow velocities are reached. Studies by Nurick[7] and Schmidt et al.[8] showed that this cavitation formation depends strongly on the nozzle geometry, and in particular, they observed that this kind of cavitation can be avoided by combining high conicity in the nozzle orifices and high hydro-grinding rates (which result in high rounding radii at the orifices inlet). The formation of this cavitation has shown to significantly affect the nozzle permeability characteristics, due to a significant decrease in the nozzle effective diameter.[9] Gavaises et al.[10] detected that string cavitation can also appear in diesel injector nozzles. This string cavitation is induced by a vortex flow created at the inlet of the nozzle orifices and can appear in both valve-covered orifice (VCO)[11] and sac nozzles,[12] although they tend to reduce as the sac volume increases. Finally, cavitation can also appear in the needle seat area when the needle is placed at low-lift conditions.[13,14]

[1]CMT-Motores Térmicos, Universitat Politècnica de València, Camino de Vera, s/n. 46022 Valencia, Spain
[2]Universidad Autónoma de Nuevo León, Facultad de Ingeniería Mecánica y Eléctrica (FIME), Laboratory for Research and Innovation in Energy Technology (LIITE), San Nicolás de los Garza, Nuevo León, México

Corresponding author:
Oscar A de la Garza, Universidad Autónoma de Nuevo León, Facultad de Ingeniería Mecánica y Eléctrica (FIME), Laboratory for Research and Innovation in Energy Technology (LIITE), Av. Universidad s/n. Ciudad Universitaria, San Nicolás de los Garza, Nuevo León, 66455, México.
Email: oscar.delagarzadl@uanl.edu.mx

Visualization techniques have been applied on transparent nozzles to better understand the characteristics of the cavitating flow. Soteriou et al.[15] saw that the cavitation region was formed as a cloud of small bubbles. Studies on real-scale geometries by Chaves et al.[16] and Arcoumanis et al.[17] detected cavitation as a set of film structures. Winklhofer et al.[18] and Payri et al.[19,20] showed that the onset of cavitation appears for cavitation number conditions lower than the mass flow collapse. Additionally, Winklhofer et al.[18] measured an increase in the flow velocity near the interphase between liquid and vapor, which is consistent with the increase in effective outlet velocity observed through momentum flux measurements at the nozzle outlet.[21] Mishra and Peles[22] detected a hysteresis phenomena associated with the onset of cavitation. Aleiferis et al.[23] and Jiang et al.[24] confirmed the influence of the fluid properties (mostly density and viscosity) on the cavitation formation. Sou and Pratama[25] found out that the appearance of cavitation was also affected by the asymmetry of the nozzle layout, since it changes the extent of the recirculation area. Recently, X-ray visualization techniques have been applied to characterize cavitation formation in metal nozzles, arriving to similar conclusions of the previous studies.[26]

In parallel to the experimental studies previously summarized, different numerical methodologies have been developed to study the details of cavitating flows. While some models predicted cavitation by means of bubbles growth based on Rayleigh–Plesset equation,[27–29] homogeneous mixture approaches are generally accepted as the most suitable for diesel nozzle modeling.[8,30,31] Such models, once validated, have been used to evaluate the influence of certain characteristics of the nozzle and injector geometry on cavitation formation, such as the orifice inclination angle,[32] the orifice conicity,[33,34] the orifice shape[35] or the off-axis needle motion.[36] Lately, numerical approaches trying to combine the simulation of cavitation inside the nozzle and the spray formation are being developed.[37]

The appearance of cavitation inside the nozzle has an impact not only on the injector hydraulic behavior but also on the spray formation. In particular, cavitation has shown to act as an enhancer of the fuel atomization.[15,38] Regarding the mixing process, Chaves et al.[16] studied the spray cone angle in non-reactive and non-evaporative conditions. Under supercavitation conditions, these authors observed an increase in the spray cone angle, which lead to a better mixing process. Other authors, such as Payri et al.,[39] Andriotis and Gavaises[40] and Boggavarapu and Ravikrishna,[41] also related the cavitating flow to an increase in the spray angle at ambient temperature conditions. Similar findings have been found for sprays injected at high temperature, but on an inert environment.[42,43] Finally, Payri et al.[42] and Benajes et al.[44] studied the spray cone angle, but now in fully realistic conditions (i.e. evaporative and reactive spray): in the first case, the increase in the spray cone angle as a consequence of the cavitation phenomenon was confirmed; while in the second case, the opposite trend was found: a lower spray cone angle under cavitating conditions, which lead to a worse mixing process. These last two studies show that the possible potential of a cylindrical nozzle (i.e. cavitating nozzle) on the mixing process is not yet clear. For this reason, the objective of the present publication is to go further in the knowledge of the effect of cavitation on the mixing process in diesel nozzles.

In order to reach the objective previously described, this article is divided into four additional sections, the contents of which will be presented now: in section "Experimental equipment," the experimental tools that will be employed in the study will be presented. The experimental and analysis methodology will be described in section "Experimental and analysis methodology." In section "Results and discussion," the results obtained about the effect of cavitation on the effective nozzle diameter, the effective injection velocity and the spray cone angle will be presented and discussed. And finally, the more relevant conclusions of the study will be summarized in the "Conclusion" section.

Experimental equipment

Nozzles

Two three-hole nozzles were used in the study, which were mounted in a piezo-electric injector holder. One of the nozzles inhibits the cavitation phenomenon (a conical nozzle with high level of hydro-grinding), whereas the other one promotes the appearance of the cavitation phenomenon (cylindrical nozzle without hydro-grinding). Both nozzles have different conicity levels. This level is quantified by the k-factor, which is defined in the following way

$$k-\text{factor} = \frac{d_{in} - d_{out}}{10} \quad (1)$$

where d_{out} is the nozzle outlet diameter and d_{in} is the nozzle inlet diameter, both in micrometers. In Table 1, the geometrical details, which were obtained through the silicone methodology,[45] are given.

Mass flow rate meter

The measurement of the instantaneous mass flow rate was carried out in a dedicated test rig,[46] which is based on the Bosch or long tube method. In this device, the pressure increase induced by the injection process is registered and post-processed to extract the information

Table 1. Geometrical details of the nozzles used in the study.

Nozzle	d_{in} (μm)	d_{out} (μm)	k-factor
Conical nozzle	135	105	3
Cylindrical nozzle	122	122	0

Table 2. Technical characteristics of the optically accessible engine.

Bore	150 mm
Stroke	170 mm
Effective stroke	108 mm
Compression ratio	22.5:1
Rotational speed	500 rpm
Total engine displacement	3000 cm^3

about the mass flow rate. Further details of this method are available in Payri et al.[47] and Bosch.[48]

Momentum flux test rig

The measurement of momentum flux was carried out in a dedicated test rig. The momentum flux was measured when the spray impacted a target attached to a piezo-electric pressure sensor localized at a distance of 5 mm from the nozzle hole.[47] The impact area is sufficiently large to ensure that all the spray impacts on this area. More details of this experimental equipment are available in Payri et al.[47]

Optically accessible engine

The optically accessible engine is a two-stroke, single-cylinder engine equipped with a cylinder head including a combustion chamber with an optical access. The technical data of this engine are given in Table 2. This experimental facility can work in two different configurations: reacting and non-reacting. In the reacting configuration, air is used as working fluid, and this configuration is used to characterize the combustion process. In the non-reactive, evaporative configuration, nitrogen is used as working fluid, and this other configuration is the one used to characterize the mixing process. More details about this experimental facility are available in Bermudez et al.[49]

Direct illumination by Mie scattering

This optical technique is based on obtaining images of a diesel spray illuminated in a direct way by a light beam generated thanks to a continuous light source. More details of the optical setup that has been used to apply this optical technique are available in Pastor et al.[50]

Single-cylinder engine

The single-cylinder engine is representative of a small automotive engine for passenger cars: it is derived from the DV6-TED4 engine from PSA Peugeot-Citroën, with four valves per cylinder. The main characteristics of this single-cylinder engine are given in Table 3.

Test fuel

Finally, all experiments were carried out with a standard diesel fuel, with a density (according to the EN ISO 12185/96 standards at 15 °C) of 842.1 kg/m^3 and a kinematic viscosity (according to EN ISO 3104/99 standards at 40 °C) of 2.820 $\times$ 10^{-6} m^2/s.

Table 3. Main technical characteristics of the single-cylinder engine DV6-TED4.

Bore	75.1 mm
Stroke	88.0 mm
Displacement volume	399 cm^3
Connecting rod length	123.8 mm
Bowl diameter	46.3 mm
Depth of bowl	14.3 mm
Compression ratio	16.5
Exhaust valve diameter	23.4 mm
Intake valve diameter	25.6 mm
Swirl number	2.15
Bowl volume	18.3 cm^3
Number of valves per cylinder	4

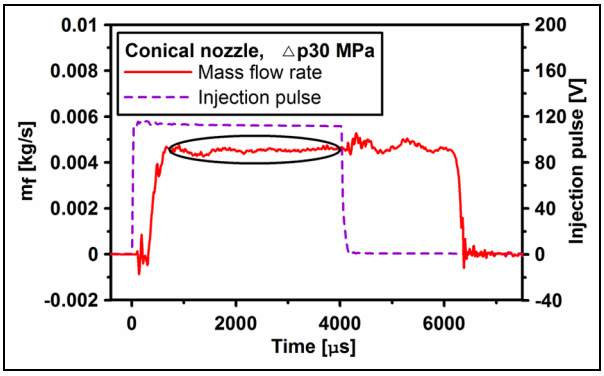

Figure 1. Example of a measurement of mass flow rate.

Experimental and analysis methodology

Hydraulic characterization

In this section, on one hand, the aspects related to the measurement of the mass flow rate and the momentum flux will be described. On the other hand, the characteristic flow parameters, which are determined with the experimental measurements previously described, will be presented.

Measurement of the mass flow rate. A mass flow meter was used to measure the mass flow rate. The measurement was carried out for long injection durations (an electric pulse of 4 ms has been used) to get a stable average value for this parameter. In Figure 1, an example of a measurement of mass flow rate, carried out with the conical nozzle, is shown. In the figure, the range (black ellipse) that has been considered to get an average value of mass flow rate is also shown.

For both nozzles, the measurements were carried out at three different levels of rail pressure (p_{rail} of 36, 76 and 146 MPa) and a single value of back pressure (p_{back} of 6 MPa). These operating conditions are representative of those existing in current diesel engines.

Measurement of momentum flux. A momentum flux test rig was used to measure this other parameter. In a

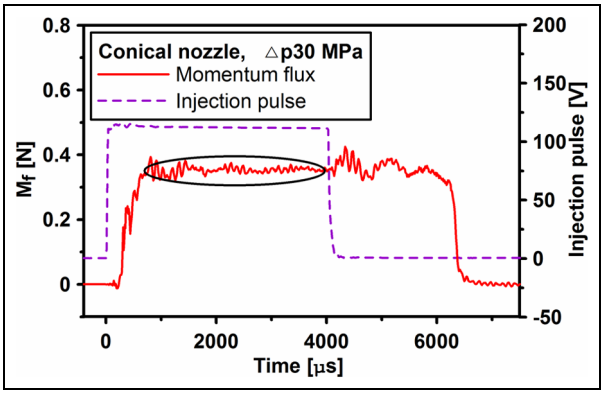

Figure 2. Example of a measurement of momentum flux.

similar way than for the mass flow rate, the measurement was carried out for long injection durations (an electric pulse of 4 ms has been used) to get a stable average value for this parameter. In Figure 2, an example of a measurement of momentum flux, carried out with the conical nozzle, is shown. In the figure the range (black ellipse) that has been considered to get an average value of momentum flux, is also shown.

In both nozzles, the measurements were carried out in the same operating conditions than for the mass flow rate to get some characteristic flow parameters that will be presented in the next section.

Characteristic flow parameters. The measurements of mass flow rate and momentum flux described previously are very useful to get some parameters that characterize the flow behavior of nozzles:[47] discharge coefficient, C_d; momentum coefficient, C_M; area coefficient, C_a and velocity coefficient, C_v. The latter one characterizes the effective injection velocity and will be used to analyze the spray cone angle calculated either from the liquid length or the heat release fraction (HRF). This is the main reason why, in the next lines, more details about the velocity coefficient will be given. However, further details about the other characteristic flow parameters are available in Payri et al.[47] The C_v is defined in the next way

$$C_v = \frac{u_{eff}}{u_{th}} \tag{2}$$

where u_{eff} is the effective injection velocity and u_{th} is the theoretical velocity, which are defined in the following way

$$u_{eff} = \frac{\dot{M}_f}{\dot{m}_f} \quad \text{and} \quad u_{th} = \sqrt{\frac{2(p_{rail} - p_{back})}{\rho_f}} \tag{3}$$

where $\dot{M}_f$ is the momentum flux, $\dot{m}_f$ is the mass flow rate and ρ_f is the fuel density. In addition, the effective area, A_{eff}, can be obtained from the experimental measurements described previously. This one is an important parameter to analyze the injection and combustion processes, as already mentioned in the "Introduction" section. In the next lines, more details about how it can be obtained will be given. On one hand, the functional dependence of the mass flow rate is defined by equation (4)

$$\dot{m}_f = \rho_f \cdot A_{eff} \cdot u_{eff} \tag{4}$$

On the other hand, the functional dependence of the momentum flux is defined by equation (5)

$$\dot{M}_f = \rho_f \cdot A_{eff} \cdot u_{eff}^2 \tag{5}$$

The combination of equations (4) and (5) leads to equation (6), which was described previously

$$u_{eff} = \frac{\dot{M}_f}{\dot{m}_f} \tag{6}$$

A_{eff} is obtained by relating equations (5) and (6) in the following way

$$A_{eff} = \frac{\dot{m}_f^2}{\dot{M}_f \cdot \rho_f} \tag{7}$$

Finally, the effective diameter, d_{eff}, is obtained from equation (7), which is defined in the next way

$$d_{eff} = \sqrt{\frac{\dot{m}_f^2 \cdot 4}{\rho_f \cdot \dot{M}_f \cdot \pi}} \tag{8}$$

Characterization of the spray cone angle

The spray cone angle is a parameter that characterizes the mixing process, as already mentioned in the "Introduction" section. It will be studied in two different scenarios: based on the liquid length (nearly realistic conditions, that is, non-reactive evaporative spray) and based on the HRF (fully realistic conditions, that is, evaporative and reactive spray). In the first scenario, two spray cone angles will be analyzed: on one hand, the one obtained through the functional dependence of the liquid length and, on the other hand, the one measured directly from the images of the liquid phase. In the second scenario, however, only the spray cone angle obtained from the functional dependence of the spray burning rate (assumed to be equivalent to the spray mixing rate) will be used.

Characterization of the spray cone angle from experiments of liquid length. The optically accessible engine and the direct illumination by Mie scattering technique were used to measure the liquid length. The image acquisition through illumination by Mie scattering is composed by a xenon light source and two optical fibers that lead a light beam until the optical access, as already mentioned in the "Direct illumination by Mie scattering" section. The operating conditions, as well as the point of injection, were the same in all the experiments carried out. Regarding the point of injection, it was at top dead centre (TDC), where the thermodynamic conditions are more stable, and at this point, the in-cylinder

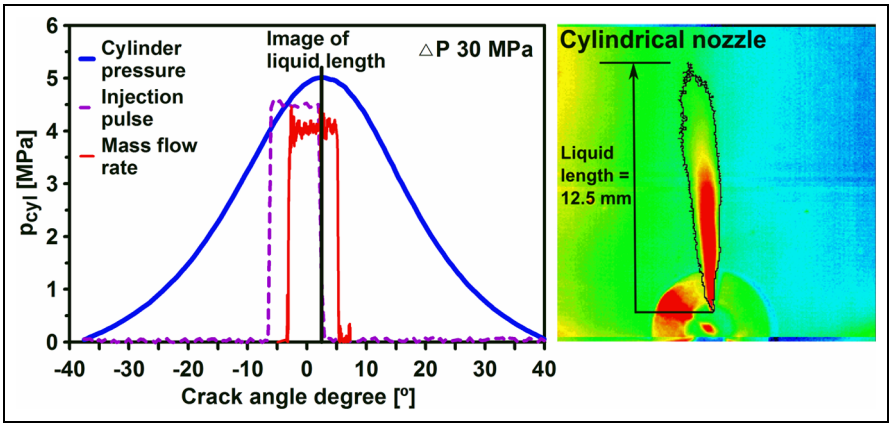

Figure 3. (Left) Position in the engine cycle of the events the most relevant for the experiment. (Right) Image of liquid length obtained with the cylindrical nozzle and with a $\Delta p = 30$ MPa ($p_{rail} = 36$ MPa $- p_{back} = 6$ MPa).[52]

temperature and density were 982 K and 21 kg/m^3, respectively. Regarding the pressures, they were 36, 76 and 146 MPa for p_{rail} and 6 MPa for p_{back}. In addition, in some cases, the p_{rail} level of 26 MPa was added.

The visualization of the liquid length was centered in one of the three nozzle orifices. In Figure 3, to the right, a sample image of liquid length is shown. The color scale of this image is arbitrary and was selected with the only purpose to better show the liquid length. The spray contour detected by the algorithm developed by Pastor et al.[51] has been added to the image of liquid length, and the value of this parameter in millimeters is also shown in the image. And in Figure 3, to the left, the position along the engine cycle of the events, the most relevant for the corresponding test, are shown (i.e. cylinder pressure, injection pulse and mass flow rate). In addition, a black, vertical line has been added to indicate the instant where the liquid length image was obtained. This image corresponds to the cylindrical nozzle, with $\Delta p = 30$ MPa ($p_{rail} = 36$ MPa $- p_{back} = 6$ MPa).

From the spray contour displayed before, the spray penetration, s, or liquid length, and the spray cone angle are measured. These two spray parameters are schematically shown in Figure 4. The spray cone angle was obtained through the least-squares fit of two straight lines from the points of the spray contour detected closer to the spray origin. For this fit, five different criteria were considered, taking into account all the points available at 15%, 30%, 45%, 60% and 75% of the spray penetration, thus giving rise to five different values for the spray cone angle. On one hand, the criterion of 15% of the spray penetration has too few points of the spray contour, and therefore, the statistic fit of the two straight lines will be little consistent. On the other hand, at the criterion of 75% of the spray penetration, the fitting of the two straight lines is carried out with almost all the points conforming the liquid spray contour, also including those already out of the conical part of the spray. For this reason, the corresponding spray cone angle will not be representative of the spray cone angle object of study. Therefore, only the cases 30%, 45% and 60% will be considered in the forthcoming analysis.

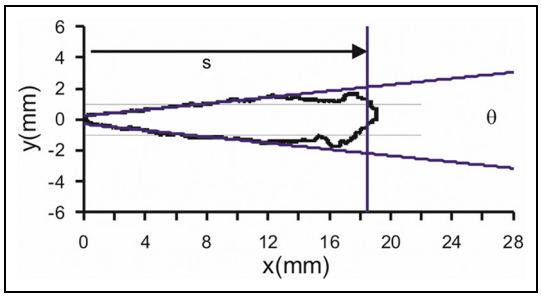

Figure 4. Representation of the parameters measured with the image processing algorithm.
Source: Adapted from García.[52]

Now, the two spray cone angles deduced from these experiments will be presented and discussed.

Spray cone angle obtained applying the functional dependence of the liquid length. The first spray cone angle will be obtained like mentioned previously, through the functional dependence of the liquid length. In Figure 5, the temporal evolution of the liquid length during an injection event is shown. In this figure, also a region is presented delimited by two vertical dashed lines, which will be used to obtain an average value of the liquid length that will be employed to analyze the results.

In Figure 6, the average values of the liquid length for each of the nozzles and p_{rail} levels studied (36, 76 and 146 MPa) are plotted versus p_{rail}. In addition, in the figure, the confidence interval is shown, taken as $\pm\sigma$, where σ is the standard deviation.

Based on the confidence intervals shown in Figure 6, it can be observed that the variation of the liquid length caused by the experimental dispersion is very similar in both nozzles and is around $\pm 5\%$. From the figure, it

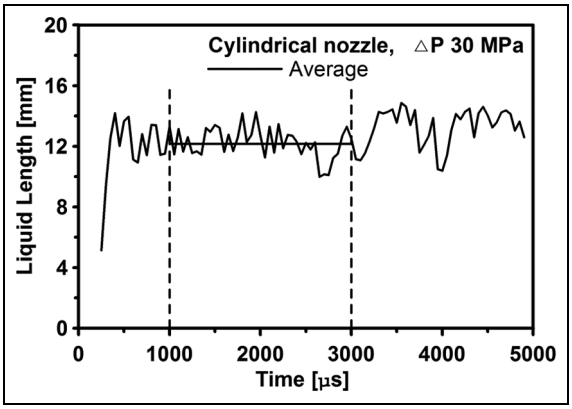

Figure 5. Temporal evolution of the liquid length during an injection event.

can be also observed that the injection pressure has no significant effect on the liquid length, which is consistent with Siebers.[53] The functional dependence of the liquid length, which will be used to extract information about the spray cone angle, is the following[54]

$$LL \propto \frac{d_{eff} \cdot \sqrt{\rho_f / \rho_a}}{Y_{f,evap} \cdot tan(\theta/2)} \tag{9}$$

where d_{eff} is the effective diameter, presented previously, and $Y_{f,evap}$ is the mass fraction of total evaporation of the fuel. This last parameter indicates when the amount of air entrained by the spray is sufficient to completely evaporate the fuel. It depends only on the thermodynamic conditions of the air and the properties of the fuel. The angle obtained from equation (9) (i.e. the functional dependence of the liquid length) will be referred as Ang_LL_F.

In Figure 7, the average values of Ang_LL_F for each of the nozzles and p_{rail} levels studied (36, 76 and 146 MPa) are shown. In addition, as in the previous figure, the confidence intervals are also shown, taken as $\pm\sigma$, where σ is the standard deviation.

From Figure 7, two aspects can be observed: on one hand, that the spray cone angle (Ang_LL_F) decreases as p_{rail} increases. And, on the other hand, that once p_{rail} is high enough (e.g. 76 and 146 MPa), the p_{rail} level do not affect the spray cone angle in a significant way. Both observations are in agreement with Naber and Siebers,[55] Desantes et al.[56] and Delacourt et al.[57]

Finally, it is worthy to note that the authors are aware that the spray cone angle obtained from the liquid length (evaporative but non-reacting spray) is surely different to the spray cone angle that will be obtained later in this article from the HRF (evaporative

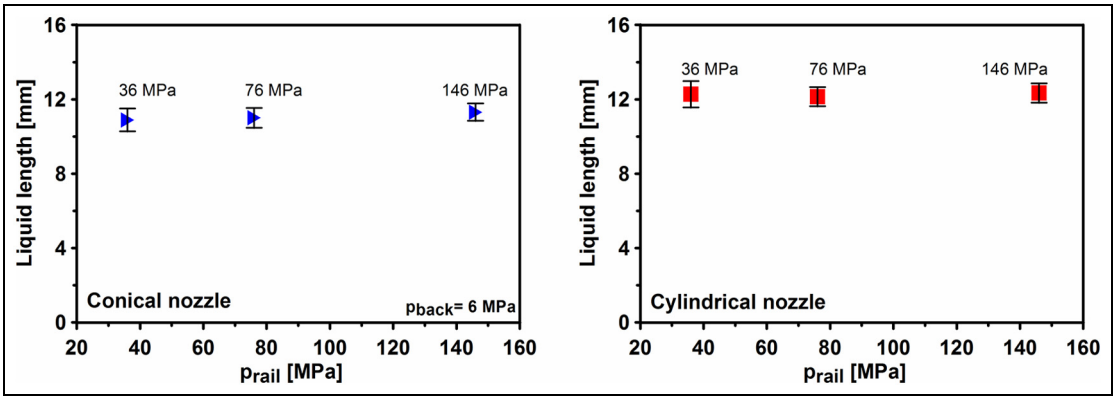

Figure 6. Evolution of the liquid length versus p_{rail}. (Left) Conical nozzle. (Right) Cylindrical nozzle.

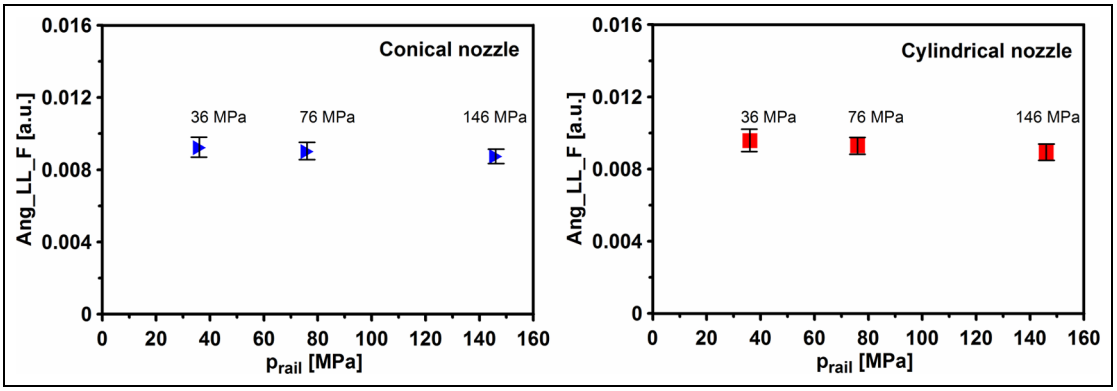

Figure 7. Evolution of Ang_LL_F versus p_{rail}. (Left) Conical nozzle. (Right) Cylindrical nozzle.

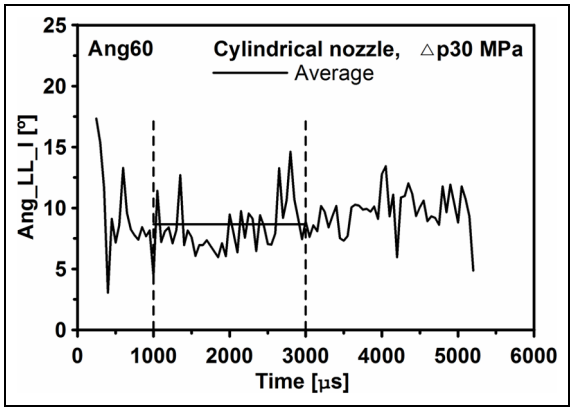

Figure 8. Evolution of Ang_LL_I (considering only the spray contour up to 60% of the spray tip penetration) during an injection event.

and reacting spray). However, these two spray cone angles should be proportional to each other. In fact, this will be confirmed by the results that will be presented in the forthcoming subsections.

Spray cone angle obtained through direct measurement from the images of liquid phase. The second spray cone angle will be obtained, as mentioned previously, through a direct measurement from the images of liquid phase. This other angle will be referred as Ang_LL_I. In Figure 8, the temporal evolution of Ang_LL_I during an injection event obtained considering only the spray contour up to 60% of the spray tip penetration is shown. In addition, in this figure, also a region is presented delimited by two vertical dashed lines, which will be used to obtain an average value of the spray cone angle that will be employed to analyze the results.

In Figure 9, the average values of Ang_LL_I for each of the nozzles and p_{rail} levels studied (26, 36, 76 and 146 MPa) are plotted versus p_{rail}. In this figure, the confidence interval is also shown. In addition, in this figure, the average values from the repetition cases (used for validation purposes) are shown: for the conical nozzle, it corresponds to p_{rail} of 36 MPa, while for the cylindrical nozzle, it corresponds to p_{rail} 26 MPa. It is worthy to note that when a sweep of p_{rail} was completed for a particular nozzle, the first pressure level was tested again with the objective of finding out, on one hand, the proper operation of the optically accessible engine and, on the other hand, the proper functioning of the high-speed camera. These repetitions indicate that both systems/equipments (the engine and the visualization system) have properly operated during the tests for both nozzles.

In Figure 9, if the attention is focused on the results obtained by application of the criterion Ang60 and for the conical nozzle, it can be seen that p_{rail} does not affect the spray cone angle, which is in agreement with Naber and Siebers,[55] Desantes et al.[56] and Delacourt et al.[57] In this figure, it can also be seen that the repetition case is very coherent for criterion Ang60, or at least more coherent than for the other criteria (Ang30 and Ang45). For these two reasons, the forthcoming analysis will be focused on the results coming from criterion Ang60 (consequently, further on, Ang_LL_I will be Ang60). In addition, the spray cone angle at 26 MPa of p_{rail} for the conical nozzle has been extrapolated from the three other pressure levels tested, with the objective of allowing the comparison with the corresponding angle of the cylindrical nozzle at this pressure level, since for this other nozzle, this pressure was included in the testing plan. In the next section, more details about the second scenario that will be employed to characterize the spray cone angle (i.e. the HRF) will be given.

Characterization of the spray cone angle from experiments of HRF. The HRF is related to the thermal energy released during the combustion process and is a function of the crank angle. This parameter is determined through an in-house combustion diagnostic model called CALMEC,[58,59] developed at CMT-Motores Térmicos. It is a zero-dimensional, single-zone model, which is based, on one hand, on the resolution of first principle of thermodynamics for an open system and, on the

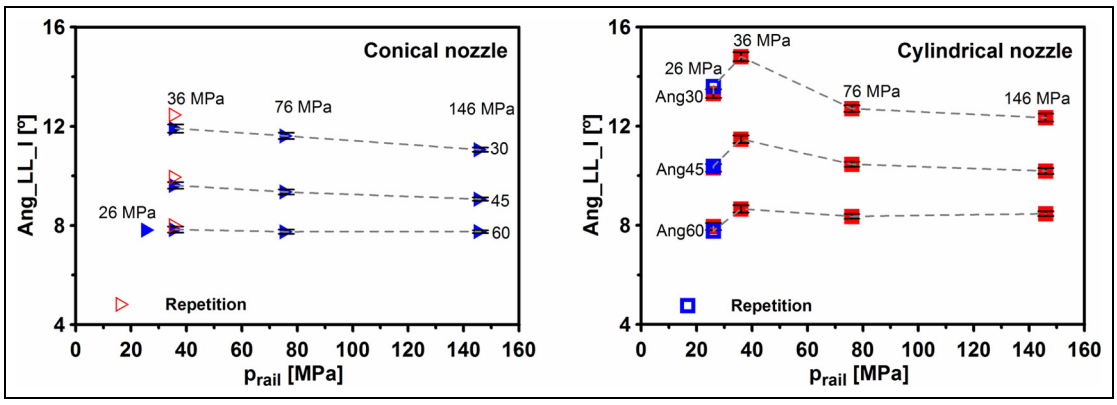

Figure 9. Evolution of Ang_LL_I (obtained from direct measurement from the spray liquid length images) versus p_{rail}. (Left) Conical nozzle. (Right) Cylindrical nozzle.

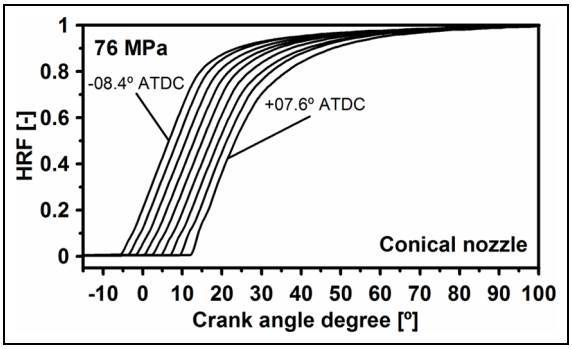

Figure 10. Evolution of the HRF (non-dimensional) versus crank angle, for different injection timings, for the conical nozzle and 76 MPa of p_{rail}.

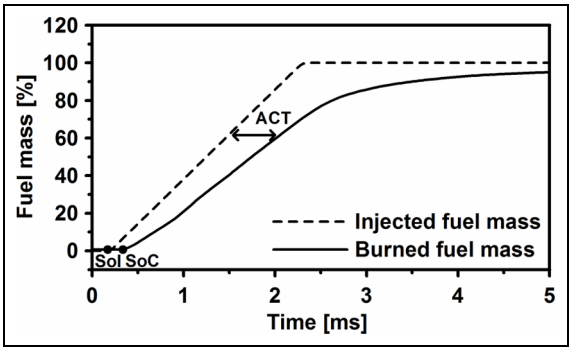

Figure 11. Injected and burned fuel mass versus time. This information is from the conical nozzle, p_{rail} level of 146 MPa and injection timing of $-0.4°ATDC$. The apparent combustion time (ACT) represents a characteristic combustion time.

other hand, on the equation of state. One of the main hypotheses assumed in this model, for simplicity reasons, is that both the pressure and temperature are uniform inside the cylinder.

The combustion diagnostic model needs several data to operate, such as the instantaneous in-cylinder pressure signal, geometrical data of the engine (bore, stroke, etc.) and of its operation (engine speed, fuel mass flow rate, etc.) and, finally, the characteristics of the fluids employed. More details about the CALMEC model are available in Lapuerta and colleagues.[58,59]

A single-cylinder engine will be used to measure the instantaneous in-cylinder pressure. Regarding the testing methodology, several aspects can be mentioned: first, the operating conditions used in the engine during the tests for the conical and the cylindrical nozzles were the same (i.e. same engine speed, intake pressure and temperature). Second, for both nozzles and p_{rail} levels (76 and 146 MPa), a sweep of injection timings was carried out, so as to modify the relative position of the combustion process in the cycle. Thanks to this methodology, a set of tests with different CA50 (the angle where 50% of the fuel mass has been burned) is available for each nozzle and p_{rail}, thus allowing the selection of cases with identical position of the combustion process in the cycle (i.e. identical CA50) for a fairer comparison. The main reason for this choice is that in two tests with the same CA50, the piston position, in average, is the same, and therefore the in-cylinder thermodynamic conditions (temperature and air density) will be the same. Third, for the two p_{rail} levels tested, the same fuel mass was injected so as to work with identical global F (fuel/air ratio) in both cases. And, finally, long injections of around 2 ms were used to ensure diffusive (i.e. mixing controlled) combustions, since it is only under these circumstances that the spray theory can be applied, which will allow extracting information about the spray cone angle.

The evolution of the instantaneous in-cylinder pressure was recorded at each of the experiments to determine the HRF through the CALMEC model. In Figure 10, the evolution of the HRF (non-dimensional)

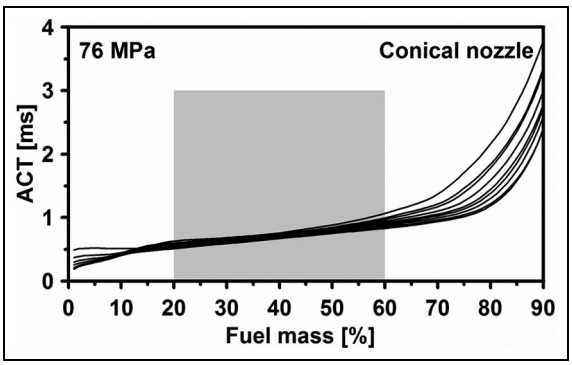

Figure 12. Evolution of the ACT parameter versus the percentage of the fuel mass, for different injection timings, for the conical nozzle and 76 MPa of p_{rail} level.

versus crank angle for different injection timings is shown. The tests were performed with the conical nozzle and a p_{rail} level of 76 MPa.

The apparent combustion time (ACT) parameter[60] will be used to analyze the mixing process. Since the combustion process is mixing controlled, because of its diffusive character, the ACT, a parameter that will be explained in the following paragraphs, can be used as an indicator of the characteristic mixing time. In Figure 11, two pieces of information are shown: on one hand, the cumulated injected fuel mass (dashed line) and, on the other hand, the burned fuel mass (continuous line), both normalized from 0% to 100% and plotted versus time. From this figure, it can be seen that the ACT parameter corresponds to the (apparent) time that the injected fuel takes to burn.

The evolution of the ACT parameter can be plotted for each nozzle, p_{rail} level and injection timing as a function of the percentage of the fuel mass. This is shown in Figure 12 for different injection timings for the conical nozzle and 76 MPa of p_{rail}. In addition, a region marked with a gray square is also shown in the figure, indicating

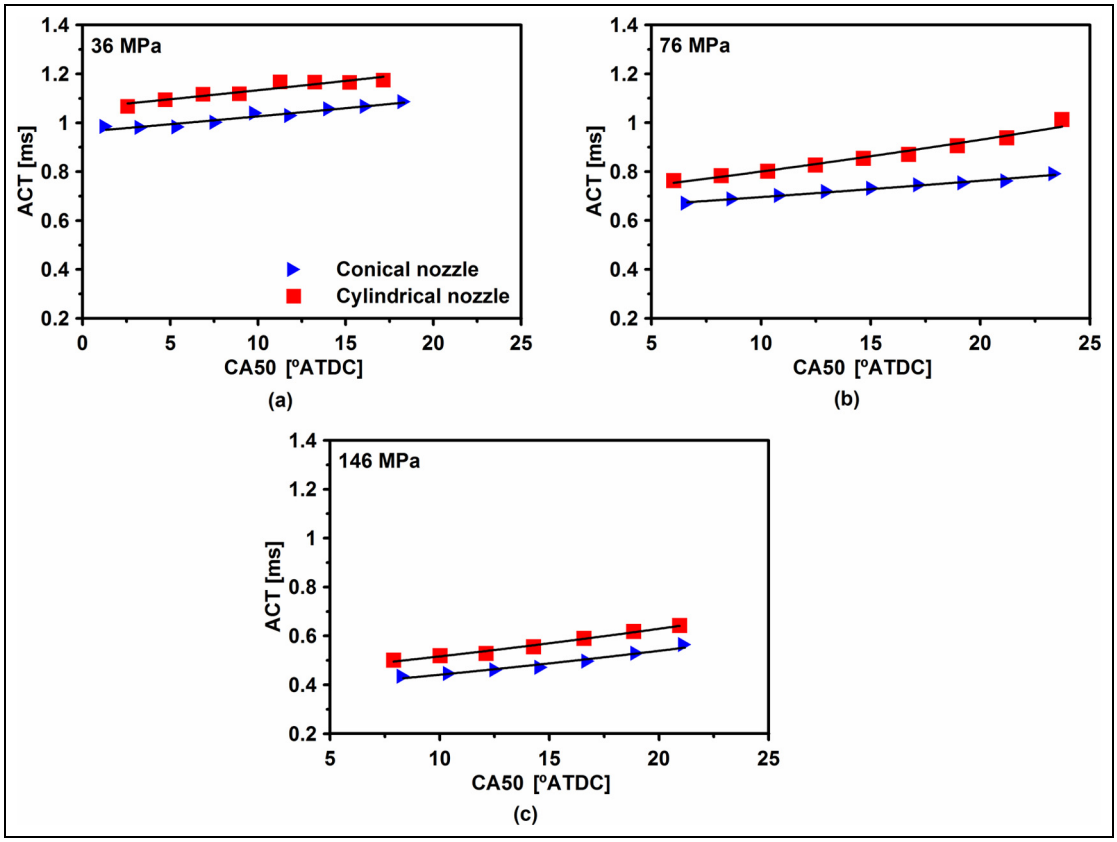

Figure 13. Average ACT versus CA50, for different injection timing for the conical and cylindrical nozzles, and p_{rail} levels of (a) 36 MPa, (b) 76 MPa and (c) 146 MPa.

the range where an average value for the ACT parameter will be computed, which later will be used to analyze the results.

In Figure 13, the average ACT for each of the injection timings, p_{rail} levels (36, 76 and 146 MPa), and nozzles studied, is plotted versus CA50 (i.e. the angle giving the combustion position in the cycle). In addition, a fitting curve for each case (nozzle and pressure) is also shown in the figure. The purpose of these fits is twofold: first, to filter the possible experimental uncertainties and, second, to allow interpolation and/or extrapolation to other values of CA50 not tested.

Now, the methodology that will be used to obtain the spray cone angle from the ACT parameter will be described.

Obtaining the spray cone angle from the ACT parameter. Equation (10) defines the characteristic mixing time obtained by application of the spray theory[61]

$$t_{mix} \propto \frac{1}{tan(\theta/2)} \cdot d_{eff} \cdot \frac{1}{u_{eff}} \cdot \left(\frac{\rho_f}{\rho_a}\right)^{\frac{1}{2}} \tag{10}$$

where t_{mix} is the characteristic mixing time, θ is the spray cone angle, d_{eff} is the effective diameter, u_{eff} is the effective injection velocity and ρ_a and ρ_f are the air and the fuel densities, respectively. It is worthy to note that t_{mix} (the characteristic mixing time) is equivalent to the ACT parameter. Therefore, equation (10) can be rewritten in the following way

$$ACT \equiv t_{mix} \propto \frac{1}{tan(\theta/2)} \cdot d_{eff} \cdot \frac{1}{u_{eff}} \cdot \left(\frac{\rho_f}{\rho_a}\right)^{\frac{1}{2}} \tag{11}$$

The cases from the conical and cylindrical nozzles will be compared at iso-CA50, to ensure that the in-cylinder thermodynamic conditions (temperature and density) are the same. Taking into account this fact, equation (11) can be simplified to the next equation

$$ACT \equiv t_{mix} \propto \frac{1}{tan(\theta/2)} \cdot d_{eff} \cdot \frac{1}{u_{eff}} \tag{12}$$

The term $tan\,(\theta/2)$ from equation (12) can be isolated, leading to equation (13)

$$tan(\theta/2) \propto \frac{d_{eff}}{u_{eff} \cdot ACT} \tag{13}$$

It is important to note that the spray cone angle obtained in this way corresponds to real conditions, that is, evaporative and reactive spray, and it will be referred as Ang_ACT further on. Now, the main results and the discussion of this study will be presented.

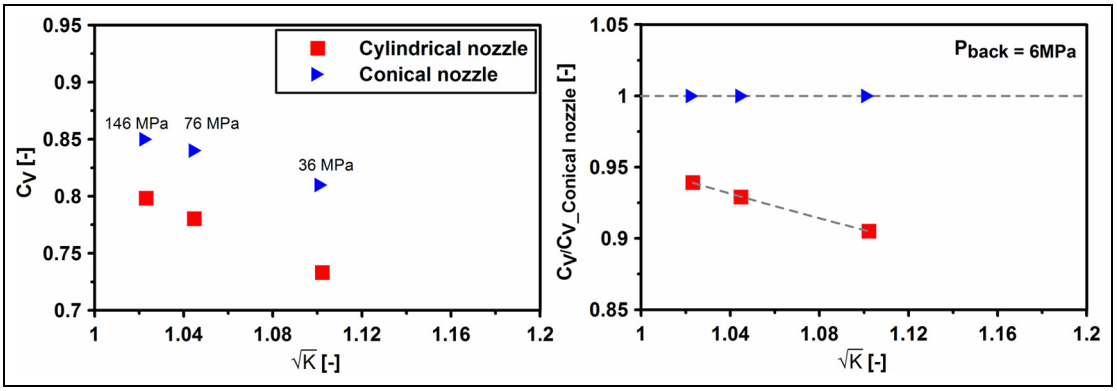

Figure 14. Evolution of C_v versus $\sqrt{K}$ for the conical and cylindrical nozzles. (Left) Values of C_v. (Right) Values of C_v normalized with the corresponding value of C_v from the conical nozzle.

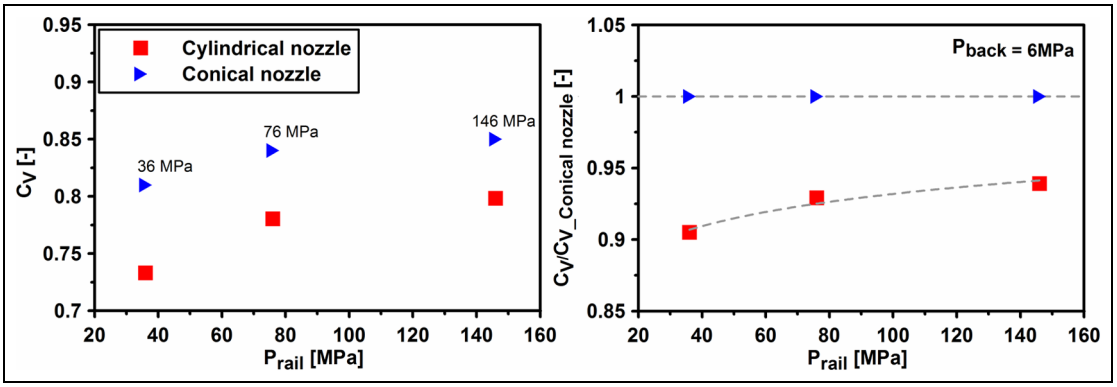

Figure 15. Evolution of C_v versus p_{rail} for the conical and cylindrical nozzles. (Left) Values of C_v. (Right) Values of C_v normalized with the corresponding value of C_v from the conical nozzle.

Results and discussion

Effect of cavitation on the effective diameter and the effective injection velocity

In Figure 14, to the left, the evolution of C_v for the conical and cylindrical nozzles versus the root square of the cavitation number ($\sqrt{K}$) is shown. In the same figure, to the right, the same information is presented, but now the values of C_v have been normalized with the corresponding value of C_v from the conical nozzle (that's the reason why all the values for the conical nozzle are 1). Also, in this way, the results of C_v are totally equivalent to those of u_{eff}. The cavitation number was proposed by Nurick[7] to quantify the cavitation level in a nozzle and is defined in the next way

$$K = \frac{p_{rail} - p_{vap}}{p_{rail} - p_{back}} \tag{14}$$

where p_{rail} is the rail pressure, p_{back} is the back pressure and p_{vap} is the vapor pressure of the fuel at the temperature existing in the nozzle.

In Figure 15, the same information from Figure 14 is presented, but plotted versus p_{rail}.

From the behavior of C_v for the cylindrical nozzle in Figure 14, to the right, two aspects can be seen: first, the C_v increases when the cavitation level increases (i.e. when $\sqrt{K}$ is reduced). This result is coherent with López et al.[21] Second, despite the increase in C_v as a consequence of cavitation, its value never reaches the one corresponding to the conical nozzle. In order to check the validity and/or the generality of this result, some other results from other studies (and, thus, from other nozzles) similar to the present one have been collected from the literature. The geometrical details of these other nozzles are given in Table 4. The reader should note that the nozzles have been organized by couples, that is, conical nozzle–cylindrical nozzle, since they will be analyzed in the same way as the two nozzles studied in this work.

Now, the analysis already performed in Figure 14 will be repeated for all the couples of nozzles from Table 4. The corresponding results are shown in Figure 16, where the information corresponding to the conical and cylindrical nozzles is presented in the same format as before: the evolution of C_v versus $\sqrt{K}$ (left) and the evolution of the normalized C_v (referred to the corresponding conical nozzle) versus $\sqrt{K}$ (right).

In Figure 16, to the right, it is observed that the behavior of C_v for all the nozzles is coherent with the one previously observed in Figure 14. Consequently,

Table 4. Geometrical details of the nozzles collected from the literature.

Source of data	Nozzle nomenclature	Type of nozzle and geometry	Sac geometry	d_{in} (μm)	d_{out} (μm)	k-factor
De la Garza[62]	Cylindrical nozzle-2	Multi-hole cylindrical	Mini-sac	147	147	0
	Conical nozzle-2	Multi-hole conical	Mini-sac	151	138	1.7
Payri et al.[3]	Cylindrical nozzle-3	Multi-hole cylindrical	Mini-sac	175	175	0
	Conical nozzle-3	Multi-hole conical	Mini-sac	176	160	1.6

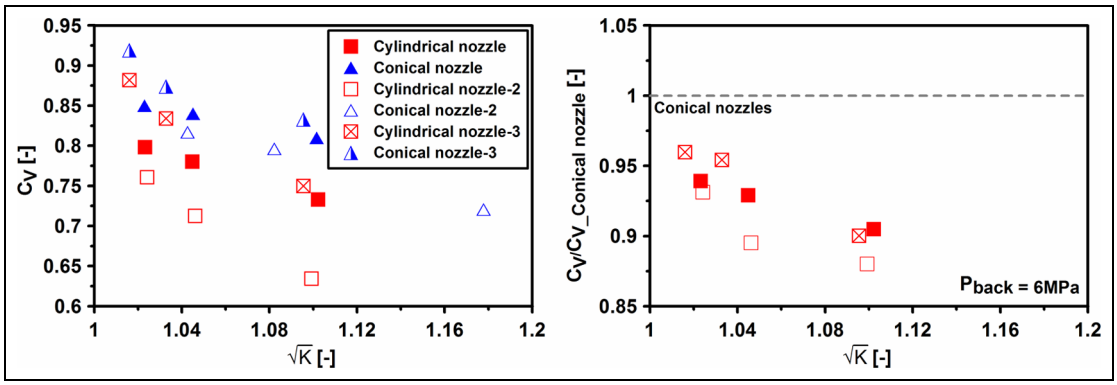

Figure 16. Evolution of C_v versus $\sqrt{K}$ for the nozzles described in Tables 1 and 4. (Left) Values of C_v. (Right) Values of C_v normalized with the corresponding value of C_v from the conical nozzle.

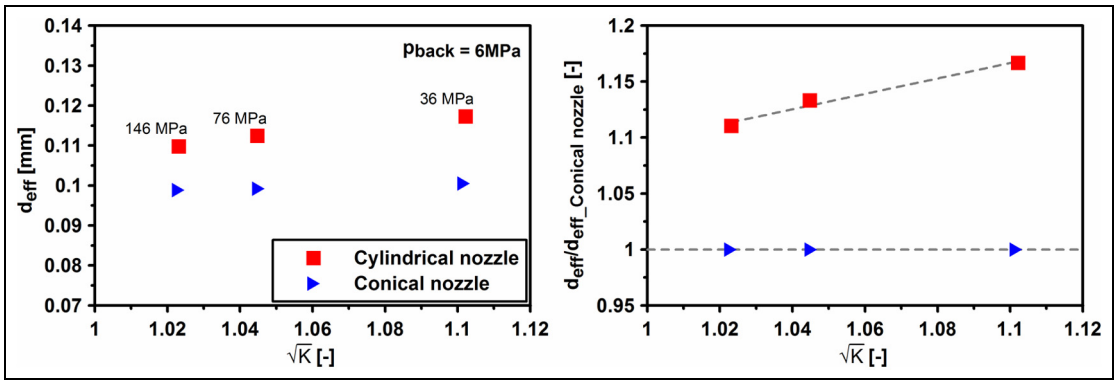

Figure 17. Evolution of d_{eff} versus $\sqrt{K}$ for the conical and cylindrical nozzles. (Left) Values of d_{eff}. (Right) Values of d_{eff} normalized with the corresponding value of d_{eff} from the conical nozzle.

two facts have been confirmed: on one hand, the increase in C_v with the increase in the cavitation level and, on the other hand, the C_v for the conical nozzle is higher compared to that for the cylindrical nozzle.

In Figure 17, to the left, the evolution of d_{eff} versus $\sqrt{K}$ for the conical and cylindrical nozzles is shown. As in the previous case, in the same figure, to the right, the same information is presented, but now the values of d_{eff} have been normalized with the corresponding value of d_{eff} from the conical nozzle.

If the trend of d_{eff} for the cylindrical nozzle in Figure 17, to the right, is studied, two aspects can be observed: first, the d_{eff} decreases with the increase in the cavitation level (i.e. when $\sqrt{K}$ is reduced). This result is consistent with the literature. And, second, the d_{eff} for the cylindrical nozzle is bigger compared to the one of the conical nozzles (between 11% and 17% higher). Therefore, the permeability of the cylindrical nozzle is higher compared to the one of the conical nozzles. It is important to remark that this is a particular result of this study. In fact, when the study was defined, the two nozzles were intended to be built with the same permeability. However, based on these results, it was not finally achieved due to a manufacturing problem. Once the behavior of the parameters d_{eff} and C_v has been studied, the effect of cavitation on the spray cone angle will be analyzed.

Effect of cavitation on the spray cone angle

As already mentioned in the "Characterization of the spray cone angle" section, the spray cone angle has

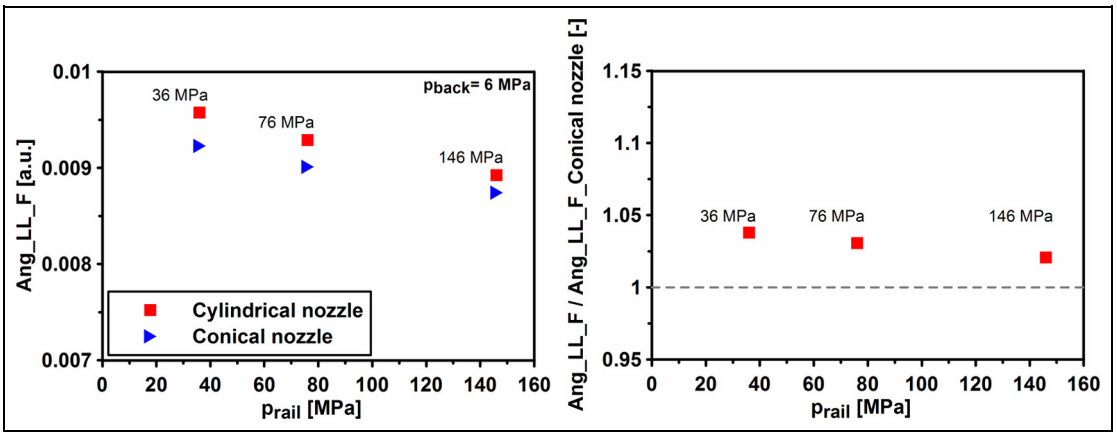

Figure 18. Evolution of Ang_LL_F versus p_{rail} for the conical and cylindrical nozzles. (Left) Values of Ang_LL_F. (Right) Values of Ang_LL_F normalized with the corresponding value of Ang_LL_F from the conical nozzle.

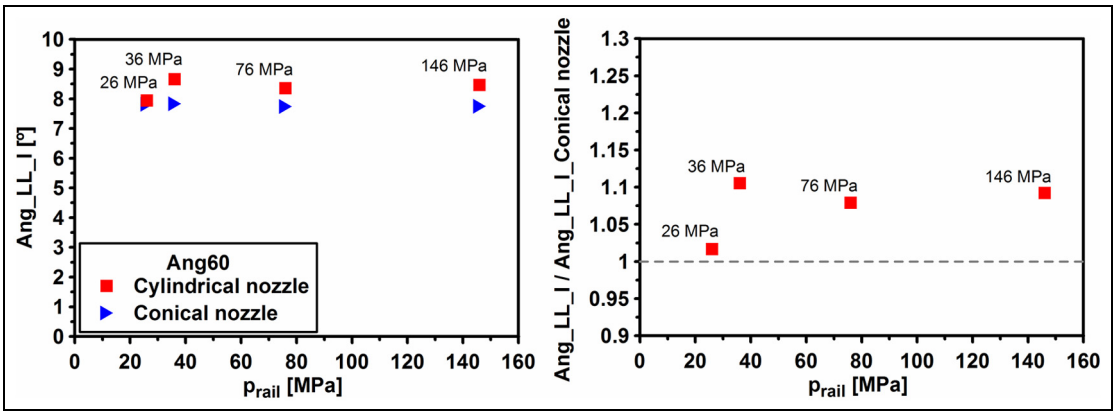

Figure 19. Evolution of Ang_LL_I versus p_{rail} for the conical and cylindrical nozzles. (Left) Values of Ang_LL_I. (Right) Values of Ang_LL_I normalized with the corresponding value of Ang_LL_I from the conical nozzle.

been characterized in two different scenarios. The first scenario was through the analysis of the images of liquid phase (near realistic conditions, that is, evaporative but non-reactive spray). As indicated previously, in this scenario, two spray cone angles will be analyzed: on one hand, it will be obtained through the functional dependence of the liquid length (Ang_LL_F) and, on the other hand, it will be obtained through direct measurement on the images of the liquid phase (Ang_LL_I). And the second scenario was to obtain the spray cone angle through the HRF, which are fully realistic conditions, that is, evaporative and reactive spray (Ang_ACT).

From the images of liquid phase. In Figure 18, to the left, the evolution of Ang_LL_F versus p_{rail} for the conical and cylindrical nozzles is shown. As already done in the previous section, in the same figure, to the right, the same information is presented, but now the values of Ang_LL_F have been normalized with the corresponding values of the conical nozzle.

Before extracting any conclusion from Figure 18, two aspects should be taken into account: first, as already mentioned previously, the experimental dispersion of the measurement of the liquid length for the conical and the cylindrical nozzles is very similar. And second, it is well known that increasing the pressure level leads to an increase in the fuel temperature, which also affects the $Y_{f,evap}$ and hence the determination of the spray cone angle. However, if the spray cone angle is analyzed at iso$-p_{rail}$ (like performed here), this problem is solved.

Taking into account these aspects, in Figure 18, to the right, it can be observed that the cylindrical nozzle has a higher spray cone angle compared to the conical nozzle for the p_{rail} levels of 36, 76 and 146 MPa, which might be caused by the cavitation phenomenon. More precisely, the average percentage of increase in spray cone angle is around 3.79%, 3.07% and 2.07%, respectively, for the p_{rail} levels of 36, 76 and 146 MPa.

In Figure 19, the results of Ang_LL_I are shown. More precisely, in the figure, to the left, the evolution of Ang_LL_I versus p_{rail} for the conical and cylindrical

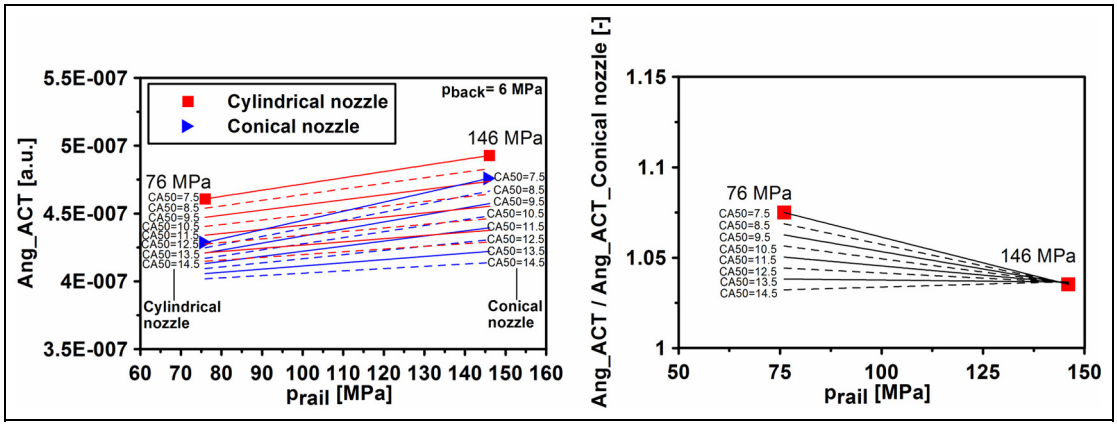

Figure 20. Evolution of Ang_ACT versus p_{rail} for the conical and cylindrical nozzles for different cases to iso-CA50. (Left) Values of Ang_ACT. (Right) Values of Ang_ACT normalized with the corresponding value of Ang_ACT from the conical nozzle.

nozzles is presented. As in the previous cases, in the same figure, to the right, the same information is presented but now the values of Ang_LL_I have been normalized with the corresponding case for the conical nozzle.

Before extracting any conclusion from the figure, it should be taken into account that the spray cone angle obtained from the images of the liquid phase is not the real spray cone angle (i.e. the corresponding to the whole spray, and consequently including both the liquid and the vapor phases), since only the liquid phase is visualized. However, both cone angles should keep a relationship (a proportionality factor). For this reason, the results illustrated in Figure 19 should be analyzed in a qualitative way.

In the figure, to the right, it can be seen that the cylindrical nozzle has a bigger Ang_LL_I compared to the conical nozzle, most probably as a consequence of the cavitation phenomenon, for the p_{rail} levels of 36, 76 and 146 MPa. However, at 26 MPa, both angles are equivalent, thus showing that there is no cavitation at these conditions, which seems reasonable. These results qualitatively show good agreement with those presented in the previous section, when the spray cone angle issued from the functional dependence of the liquid length was analyzed. In the upcoming section, the effect of cavitation on the spray cone angle obtained from the HRF will be analyzed.

From the HRF. In Figure 20, to the left, the evolution of Ang_ACT (referred to the spray cone angle obtained from the HRF) versus p_{rail} for the conical and cylindrical nozzles is shown at different CA50 (CA50 = 7.5°, 8.5°, 9.5°, 10.5°,11.5°, 12.5°, 13.5° and 14.5°). As already usual in this work, in the figure, to the right, the same information is presented, but now the values of Ang_ACT have been normalized by the corresponding values of the conical nozzle. In this figure, it can be seen that the cylindrical nozzle shows a larger spray cone angle compared to the conical nozzle as a consequence of the cavitation phenomenon. More specifically, the average percentage of increase in spray cone angle for the cases at CA50 = 11.5° (the average value of all the CA50 cases shown in the figure), is around 5.0% and 3.6%, respectively, for the cases with a p_{rail} of 76 and 146 MPa.

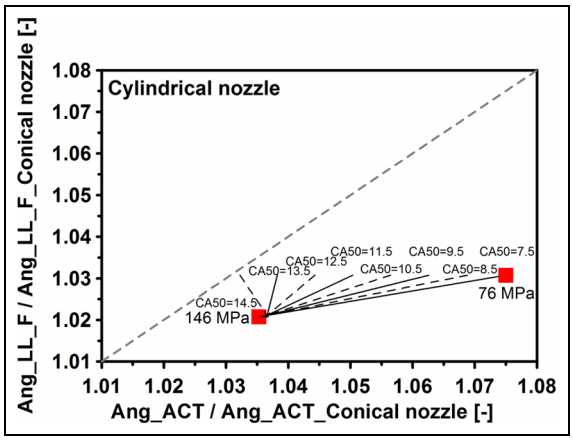

Figure 21. Evolution of Ang_LL_F versus Ang_ACT for the cylindrical nozzle for different cases at iso-CA50. The values have been normalized with the corresponding one for the conical nozzle.

In Figure 21, the results shown in Figures 18 and 20 are synthesized. Specifically, the evolution of the normalized Ang_LL_F versus the normalized Ang_ACT for the cylindrical nozzle for different cases at iso-CA50 is presented. From this figure, two aspects can be mentioned: (1) the results obtained from the functional dependence of the liquid length qualitatively show good agreement with those obtained from the HRF (a bisecting line has been included in the plot as an indication of a perfect match between the two angle definitions) and (2) the quantitative difference between these results was expected, since now experiments have been carried out in fully realistic conditions (i.e. evaporative and reactive spray).

Table 5. Comparison of the increase in spray cone angle, obtained from the liquid length (cases (a) and (b)) and from the heat release fraction (case (c)).

P_{rail} (MPa)	Increase in spray cone angle (%)		
	Case (a)	Case (b)	Case (c)
76	3.0	7.9	5.0
146	2.0	9.2	3.6

A final remark is that even though this procedure to calculate the spray cone angle is, by far, more complex compared to the procedure used in the previous section, it is obtained in fully realistic conditions and involves less inaccuracies than the other method, and the values obtained for this case are more or less an average value of all the values obtained with the different methods. Therefore, these last results (from the HRF) will be chosen to be used in the final analysis. In the next section, a synthesis of the results obtained about the mixing process in the two different scenarios (i.e. non-reacting and reacting) will be carried out.

Synthesis of the results obtained about spray cone angle. In Table 5, a comparison of the different increments in spray cone angle obtained in the previous sections is shown: (a) from the liquid length and applying its functional dependence (Ang_LL_F), (b) from a direct measurement from the images of the liquid phase (Ang_LL_I) and (c) from the HRF (Ang_ACT), in all cases for the p_{rail} levels of 76 and 146 MPa.

From this table, two conclusions can be extracted: on one hand, that the results obtained about the spray cone angle are all qualitatively consistent and, on the other hand, that there are significant differences (quantitatively speaking) between the values obtained from the different methods. These quantitative differences between the two analyzed scenarios, as mentioned previously, were already expected because of two reasons: first, because the conditions used in each of the scenarios were different (in one of the scenarios, an evaporative but non-reacting spray was analyzed, while in the other, an evaporative and reacting spray was considered). And, second, because of the significant differences in the procedure used at each scenario to determine the spray cone angle.

Now an effort will be done to try to link two of the conclusions previously described in this work: on one hand, that the u_{eff} from the cylindrical nozzle increases with the increase in the cavitation level, but never reaching the u_{eff} from the conical nozzle and, on the other hand, that the spray cone angle of the cylindrical nozzle is higher compared to the conical nozzle, also as a consequence of cavitation. From these two observations, it can be stated that the wider spray cone angle at the cylindrical nozzle is not due to an increase in u_{eff}, but most probably to the biphasic flow inside the nozzle hole. This statement is consistent with the conclusion achieved by several authors, as for instance, Kent and Brown[63] and Chehroudi et al.,[64] who concluded that the injection pressure, which is closely related to the u_{eff}, has an effect practically negligible on the spray cone angle.

In summary, the cylindrical nozzle compared to the conical nozzle and for the p_{rail} levels of 76 (medium level of cavitation) and 146 MPa (high level of cavitation) presents, on one hand, a u_{eff} lower of around 7.0% and 6.0%, respectively, for the p_{rail} levels of 76 and 146 MPa, and on the other hand, an increase in spray cone angle (Ang_ACT) of around 5.0% and 3.6%, respectively. It is worthy to point out that these last results correspond to the second scenario employed for the characterization of the spray cone angle, that is, from the HRF, since it is obtained in fully realistic conditions and involves less inaccuracies than the other method, and the values obtained for this case are more or less an average value of all the values obtained with the different methods.

Once this point is reached, a question arises, which parameter does have more influence on the mixing process, the variation of u_{eff} or the variation of the spray cone angle, both as a consequence of cavitation? To give an answer to this question, the influence of the variations of u_{eff} and the spray cone angle on the ACT parameter for p_{rail} levels of 76 and 146 MPa for the cylindrical and the conical nozzles will be analyzed. To do so, the following expression of the ACT parameter, derived from equation (13), will be used

$$ACT \propto \left(\frac{1}{u_{eff} \cdot tan(\theta/2)} \right) \tag{15}$$

From equation (15) and taking into account the results obtained during the comparison of the cylindrical with the conical nozzle, it can be said:

- At the p_{rail} level of 76 MPa, a reduction in $u_{eff}(C_v)$ of a factor of 0.929, that is, 7.1%, and an increase in spray cone angle of a factor of 1.05, that is, 5%. The combined influence on the mixing time (i.e. the ACT parameter) is an increase in a factor of 1.025, that is, 2.5%.
- At the p_{rail} level of 146 MPa, a reduction in $u_{eff}(C_v)$ of a factor 0.939, that is, 6.1%, and an increase in spray cone angle of a factor of 1.036, that is, 3.6%. The combined influence on the mixing time is an increase in a factor of 1.028, that is, 2.8%.

Therefore, analyzing on a whole, the variation of u_{eff} and the spray cone angle when comparing the cylindrical nozzle with the conical one, for the cases studied here, it is found that the mixing process worsens with the cylindrical nozzle.

Conclusion

This work has intended to deepen the knowledge about the influence of cavitation on the mixing process in diesel nozzles through the study of the influence of cavitation on the effective diameter, the effective injection velocity and the spray cone angle, parameters that affect the mixing process. The spray cone angle was studied in two different scenarios. The first scenario was based on images of the liquid phase (nearly realistic conditions, that is, evaporative but non-reactive spray). In this scenario, two spray cone angles were analyzed: on one hand, the spray cone angle obtained through the functional dependence of the liquid length and, on the other hand, the spray cone angle obtained through the direct measurement from the images of the liquid phase. The second scenario, however, was based on the HRF (fully realistic conditions, that is, evaporative and reactive spray). It is worthy to indicate that the studies available in the literature related to characterization of the spray cone angle in fully realistic conditions, that is, evaporative and reactive spray, are very scarce. Now, the main conclusions of the study will be summarized.

Regarding the effective diameter and the effective injection velocity, for the cylindrical nozzle, the reduction in the effective diameter and the increase in the effective injection velocity, both as a consequence of cavitation, were confirmed. However, despite the increase in u_{eff}, this parameter never reaches the corresponding value of the conical nozzle. Based on the information collected from the literature, this statement is consistent.

Concerning the spray cone angle, the increase in spray cone angle as a consequence of cavitation has been confirmed in both analyzed scenarios, even if there is a significant difference in the values obtained of around 4% between the two. This difference, however, was already expected because of the following two main reasons: first, because the conditions used in each of the scenarios were different (in the first scenario an evaporative but non-reactive spray was analyzed, whereas in the other an evaporative and reactive spray was studied), and second, because of the significant differences in the procedure used to determine the spray cone angle at each scenario.

The increase in spray cone angle caused by cavitation cannot be due to an increase in u_{eff}, since it is lower for the cavitating nozzle. The explanation of this increase in spray cone angle might be the biphasic flow inside the nozzle hole. However, the validation of this hypothesis will require additional research, and it is out of the scope of the present publication.

The reduction of the effective diameter, the increase in the effective injection velocity and the increase in the spray cone angle, all of them as a consequence of cavitation, lead to a better mixing process with respect to the case with no cavitation when working with a given nozzle. However, if the mixing process between the two nozzles is compared, for the cases studied here, it worsens with the cylindrical nozzle despite the benefits associated with the cavitation phenomenon mentioned previously.

Acknowledgements

The authors thank Gabriel Alcantarilla, who is a member of the CMT-Motores Térmicos team, for his support in carrying out the experimental measurements in the single-cylinder engine and also thank José María Bordes for his contribution to the work.

Declaration of conflicting interests

The author(s) declared no potential conflicts of interest with respect to the research, authorship and/or publication of this article.

Funding

The author(s) disclosed receipt of the following financial support for the research, authorship, and/or publication of this article: The authors thank the FPU program of the Spanish Ministry of Education for supporting the PhD studies of Oscar A de la Garza (grant: AP2008-01913) and also thank the PSA Peugeot-Citroën, National Council of Science and Technology (CONACYT) of the Mexican Government (project: CB-239943) and the Royal Academy of Engineering, United Kingdom (project: NRCP/1415/238) for supporting this research.

References

1. Karra PK and Kong SC. Experimental study on effects of nozzle hole geometry on achieving low diesel engine emissions. *J Eng Gas Turb Power* 2009; 132: 022802–022810.
2. Som S, Ramirez AI, Longman DE and Aggarwal S. Effect of nozzle orifice geometry on spray, combustion, and emission characteristics under diesel engine conditions. *Fuel* 2011; 90: 1267–1276.
3. Payri R, Salvador FJ, Gimeno J and Zapata LD. Diesel nozzle geometry influence on spray liquid-phase fuel penetration in evaporative conditions. *Fuel* 2008; 87: 1165–1176.
4. Wang X, Huang Z, Zhang W, Kuti OA and Nishida K. Effects of ultra injection pressure and micro-hole nozzle on flame structure and soot formation of impinging diesel spray. *Appl Energ* 2011; 88: 1620–1628.
5. Watanabe H, Nishikori M, Hayashi T, Suzuki M, Kakehashi N and Ikemoto M. Visualization analysis of relationship between vortex flow and cavitation behavior in diesel nozzle. *Int J Engine Res* 2015; 16: 5–12.
6. Hayashi T, Suzuki M and Ikemoto M. Effects of internal flow in a diesel nozzle on spray combustion. *Int J Engine Res* 2013; 14: 646–653.
7. Nurick WH. Orifice cavitation and its effects on spray mixing. *J Fluid Eng* 1976; 98: 681–687.

8. Schmidt DP, Rutland CJ and Corradini ML. *A numerical study of cavitating flow through various nozzle shapes*. SAE paper no. 971597, 1 May 1997. Warrendale, PA: SAE International.
9. Payri F, López JJ, Garcia A, De la, Garza OA and Houille S. *Effects of cavitation in common-rail diesel nozzles on the soot formation process*. SAE paper no. 2013-01-1602, 8 April 2013. Warrendale, PA: SAE International.
10. Gavaises M, Andriotis A, Papoulias D, Mitroglou N and Theodorakakos A. Characterization of string cavitation in large-scale diesel nozzles with tapered holes. *Phys Fluids* 2009; 21(5): 052107.
11. Reid BA, Hargrave GK, Garner CP and Wigley G. An investigation of string cavitation in a true-scale fuel injector flow geometry at high pressure. *Phys Fluids* 2010; 22: 031703.
12. Mitroglou N and Gavaises M. Mapping of cavitating flow regimes in injectors for medium-/heavy-duty diesel engines. *Int J Engine Res* 2013; 14(6): 590–605.
13. Mitroglou N, McLorn M, Gavaises M, Soteriou C and Winterbourne M. Instantaneous and ensemble average cavitation structures in diesel micro-channel flow orifices. *Fuel* 2014; 116: 736–742.
14. Desantes JM, Salvador FJ, Carreres M and Martínez-López J. Large-eddy simulation analysis of the influence of the needle lift on the cavitation in diesel injector nozzles. *Proc IMechE, Part D: J Automobile Engineering* 2014; 229(4): 407–423.
15. Soteriou C, Andrews R and Smith M. *Direct injection diesel spray and the effect of cavitation and hydraulic flip on atomization*. SAE paper no. 950080, 1 February 1995. Warrendale, PA: SAE International.
16. Chaves H, Knapp M and Kubizek A. *Experimental study of cavitation in the nozzle hole of diesel injectors using transparent nozzles*. SAE paper no. 950290, 1 February 1995. Warrendale, PA: SAE International.
17. Arcoumanis C, Flora H, Gavaises M and Badami M. *Cavitation in real-size multi-hole diesel injector nozzles*. SAE paper no. 2000-01-1249, 6 March 2000. Warrendale, PA: SAE International.
18. Winklhofer E, Kull E, Kelz E and Morozov A. *Comprehensive hydraulic and flow field documentation in model throttle experiments under cavitation conditions*. Zurich: ILASS-Europe, 2001.
19. Payri R, Salvador FJ, Gimeno J and De la Morena J. Study of cavitation phenomena based on a technique in a liquid pressurized chamber. *Int J Heat Fluid Fl* 2009; 30: 768–777.
20. Payri R, Salvador FJ, Gimeno J and Venegas O. Study of cavitation phenomenon using different fuels in a transparent nozzle by hydraulic characterization and visualization. *Exp Therm Fluid Sci* 2013; 44: 235–244.
21. López JJ, Salvador FJ, De la Garza OA and Arregle J. A comprehensive study on the effect of cavitation on injection velocity in a diesel nozzle. *Energ Convers Manage* 2012; 64: 415–423.
22. Mishra C and Peles Y. Flow visualization of cavitating flows through a rectangular slot micro-orifice ingrained in a microchannel. *Phys Fluids* 2005; 17(11): 113602.
23. Aleiferis PG, Serras-Pereira J, Augoye A, Davies TJ, Cracknell RF and Richardson D. Effect of fuel temperature on in-nozzle cavitation and spray formation of liquid hydrocarbons and alcohols from a real-size optical injector for direct-injection spark-ignition engines. *Int J Heat Mass Tran* 2010; 53(21–22): 4588–4606.
24. Jiang G, Zhang Y, Wen H and Xiao G. Study of the generated density of cavitation inside diesel nozzle using different fuels and nozzles. *Energ Convers Manage* 2015; 103: 208–217.
25. Sou A and Pratama RH. Effects of asymmetric inflow on cavitation in fuel injector and discharged liquid jet. *Atomization Spray* 2016; 26(9): 939–959.
26. Duke DJ, Swantek AB, Tilocco Z, Kastengren AL, Fezzaa K, Neroorkar K, et al. *X-ray imaging of cavitation in diesel injectors*. SAE paper no. 2014-01-1404, 1 April 2014. Warrendale, PA: SAE International.
27. Yuan W and Schnerr GH. Numerical simulation of two-phase flow in injection nozzles: interaction of cavitation and external jet formation. *J Fluid Eng* 2003; 125(6): 963–969.
28. Alajbegovic A, Meister G, Greif D and Basara B. Three phase cavitating flows in high-pressure swirl injectors. *Exp Therm Fluid Sci* 2002; 26: 677–681.
29. Som S, Longman DE, Ramírez AI and Aggarwal SK. A comparison of injector flow and spray characteristics of biodiesel with petrodiesel. *Fuel* 2010; 89: 4014–4024.
30. Peng Kärrholm F. *Numerical modelling of diesel spray injection, turbulence interaction and combustion*. PhD Thesis, Chalmers University of Technology, Gothenburg, 2008.
31. Habchi C, Dumont N, Simonin O, Soteriou C, Torres N and Andrews R. Multidimensional simulation of cavitating flows in diesel injectors by a homogeneous mixture modeling approach. *Atomization Spray* 2008; 18: 129–162.
32. De la, Morena J, Neroorkar K, Plazas AH, Peterson RC and Schmidt DP. Numerical analysis of the influence of diesel nozzle design on internal flow characteristics for 2-valve diesel engine application. *Atomization Spray* 2013; 23(2): 97–118.
33. Brusiani F, Falfari S and Pelloni P. Influence of the diesel injector hole geometry on the flow conditions emerging from the nozzle. *Energy Procedia* 2014; 45: 749–758.
34. Mohan B, Yang W and Chou SK. Cavitation in injector nozzle holes: a parametric study. *Eng Appl Comp Fluid* 2014; 8(1): 70–81.
35. Molina S, Salvador FJ, Carreres M and Jaramillo D. A computational investigation on the influence of the use of elliptical orifices on the inner nozzle flow and cavitation development in diesel injector nozzles. *Energ Convers Manage* 2014; 79: 114–127.
36. Battistoni M, Xue Q, Som S and Pomraning E. Effect of off-axis needle motion on internal nozzle and near exit flow in a multi-hole diesel injector. *SAE Int J Fuel Lubr* 2014; 7(1): 167–182.
37. Xue Q, Battistoni M, Powell CF, Longman DE, Quan S, Pomraning E, et al. An Eulerian CFD model and X-ray radiography for coupled nozzle flow and spray in internal combustion engines. *Int J Multiphas Flow* 2015; 70: 77–88.
38. Suh HK and Lee CS. Effect of cavitation in nozzle orifice on the diesel fuel atomization characteristics. *Int J Heat Fluid Fl* 2008; 29: 1001–1009.
39. Payri R, Molina S, Salvador FJ and Gimeno J. A study of the relation between nozzle geometry, internal flow and sprays characteristics in diesel fuel injection systems. *KSME Int J* 2004; 18: 1222–1235.

40. Andriotis A and Gavaises M. Influence of vortex flow and cavitation on near-nozzle diesel spray dispersion angle. *Atomization Spray* 2009; 19(3): 247–261.
41. Boggavarapu P and Ravikrishna RV. A comparison of diesel and jatropha methyl ester (JME) spray characteristics: effect of nozzle entry radius. *Atomization Spray* 2016; 26(10): 961–982.
42. Payri F, Arregle J, López JJ and Hermens S. *Effect of cavitation on the nozzle outlet flow, spray and flame formation in a diesel engine*. SAE paper no. 2006-01-1391, 3 April 2006. Warrendale, PA: SAE International.
43. Westlye FR, Battistoni M, Skeen SA, Manin J, Pickett LM and Ivarsson A. *Penetration and combustion characterization of cavitating and non-cavitating fuel injectors under diesel engine conditions*. SAE paper no. 2016-01-0860, 5 April 2016. Warrendale, PA: SAE International.
44. Benajes J, Molina S, Gonzalez C and Donde R. The role of nozzle convergence in diesel combustion. *Fuel* 2008; 87: 1849–1858.
45. Macian V, Bermudez V, Payri R and Gimeno J. New technique for determination of internal geometry of diesel nozzle with the use of silicone methodology. *Exp Techniques* 2003; 27: 39–43.
46. Desantes JM, Arregle J, López JJ and Hermens S. *Experimental characterization of outlet flow for different diesel nozzle geometries*. SAE paper no. 2005-01-2120, 11 May 2005. Warrendale, PA: SAE International.
47. Payri R, Garcia JM, Salvador FJ and Gimeno J. Using spray momentum flux measurement to understand the influence of diesel nozzle geometry on spray characteristics. *Fuel* 2005; 84: 551–561.
48. Bosch W. *The fuel rate indicator: a new measuring instrument for display of the characteristics of individual injection*. SAE paper no. 660749, 1 February 1966. Warrendale, PA: SAE International.
49. Bermudez V, Garcia JM, Juli E and Martinez S. *Engine with optically accessible cylinder head: a research tool for injection and combustion process*. SAE paper no. 2003-01-1110, 3 March 2003. Warrendale, PA: SAE International.
50. Pastor JV, Payri R, Garcia-Olivier JM and Briceno FJ. Analysis of transient liquid and vapor phase penetration for diesel sprays under variable injection conditions. *Atomization Spray* 2011; 21: 503–520.
51. Pastor JV, Arregle J and Palomares A. Diesel spray images segmentation using a likelihood ratio test. *Appl Optics* 2001; 40: 2876–2885.
52. García JM. *Contribution to the study of turbulent combustion of DI diesel engine sprays*. PhD Thesis, Universitat Politècnica de València, València, 2004 (in Spanish).
53. Siebers DL. *Liquid-phase fuel penetration in diesel sprays*. SAE paper no. 980809, 23 February 1998. Warrendale, PA: SAE International.
54. Desantes JM, López JJ, Garcia JM and Pastor JM. Evaporative diesel spray modeling. *Atomization Spray* 2007; 17: 193–231.
55. Naber JD and Siebers DL. *Effects of gas density and vaporization on penetration and dispersion of diesel sprays*. SAE paper no. 960034, 1 February 1996. Warrendale, PA: SAE International.
56. Desantes JM, Pastor JV, Payri R and Pastor JM. Experimental characterization of internal nozzle flow and diesel spray behavior. Part II: evaporative conditions. *Atomization Spray* 2005; 15: 517–543.
57. Delacourt E, Desmet B and Besson B. Characterization of very high pressure diesel sprays using digital imaging techniques. *Fuel* 2005; 84: 859–867.
58. Lapuerta M, Armas O and Hernandez J. Diagnostic of DI diesel combustion from in-cylinder pressure signal by estimation of mean thermodynamic properties of the gas. *Appl Therm Eng* 1999; 19: 513–529.
59. Lapuerta M, Armas O and Bermudez V. Sensitivity of diesel engine thermodynamic cycle calculation to measurement errors and estimated parameters. *Appl Therm Eng* 2000; 20: 843–861.
60. Arregle J, López JJ, Garcia JM and Fenollosa C. Development of zero-dimensional diesel combustion model. Part I: analysis of the quasi-steady diffusion combustion phase. *Appl Therm Eng* 2003; 23: 1301–1317.
61. Desantes JM, Arregle J, López JJ and Cronhjort A. Scaling laws for free turbulent gas jets and diesel-like sprays. *Atomization Spray* 2006; 16: 443–473.
62. De la Garza OA. *Study on the effects of cavitation in diesel injection nozzles on the injection and soot formation processes*. Barcelona: Editorial Reverté, 2015 (in Spanish).
63. Kent JC and Brown GM. Nozzle exit flow, characteristics for square-edged and rounded inlet geometries. *Combust Sci Technol* 1983; 30: 121–132.
64. Chehroudi B, Chen S, Bracco F and Onuma Y. *On the intact core of full-cone sprays*. SAE paper no. 850126, 1 February 1985. Warrendale, PA: SAE International.

Appendix 1

Notation

A	area
Ang30	angle obtained considering only the spray contour up to 30% of the spray tip penetration
Ang45	angle obtained considering only the spray contour up to 45% of the spray tip penetration
Ang60	angle obtained considering only the spray contour up to 60% of the spray tip penetration
Ang_ACT	spray cone angle obtained from the heat release fraction
Ang_LL_F	spray cone angle obtained from the functional dependence of the liquid length
Ang_LL_I	spray cone angle obtained from direct measurement with the images of liquid phase
C_a	area coefficient
CA50	angle where 50% of the fuel mass has been burned
C_d	discharge coefficient
C_M	momentum coefficient
C_v	velocity coefficient
d	diameter
F	fuel/air ratio
K	cavitation number from Nurick $\left(\frac{p_{inj}-p_{vap}}{p_{inj}-p_{back}}\right)$

LL	liquid length
$\dot{m}$	mass flow rate
$\dot{M}$	momentum flux
p	pressure
s	spray penetration
SoC	start of combustion
SoI	start of injection
t	time
u	velocity
Y	mass fraction
Δ	increase
θ	spray cone angle
ρ	density
σ	standard deviation

Subscripts

a	air
$back$	volume where the fuel is injected
cyl	cylinder
eff	effective
f	fuel
$f, evap$	evaporation of fuel
in	inlet of the nozzle hole
mix	mixing
out	outlet of the nozzle hole
$rail$	common rail
th	Bernoulli (theoretical)
vap	fuel vapor